ACS Macro Letters

Letter

pubs.acs.org/macroletters

Aerosol-Processed Thermosensitive Nanocomposites for Controlled Drug Release

Jeong Hoon Byeon*,† and Jang-Woo Kim*,‡

†Department of Chemistry, Purdue University, West Lafayette, Indiana 47907, United States

‡Department of Digital Display Engineering, Hoseo University, Asan 336-795, Republic of Korea

Supporting Information

ABSTRACT: In this study, an ambient-spark-produced iron (Fe)-nanoparticle-laden nitrogen gas was mixed with an atomized solution of *N*-isopropylacrylamide (NIPAM)-polydimethylsiloxane (PDMS). The Fe nanoparticles reacted with NIPAM-PDMS in the atomized droplets to form encapsulated Fe nanoparticles, i.e., Fe@NIPAM-PDMS nanocomposites, whose size distribution was unimodal (showing only a NIPAM-PDMS-like distribution, with the Fe distribution eliminated). By varying processing temperatures, it was possible to obtain Fe@NIPAM-PDMS nanocomposites with different sizes and morphologies. This is further attributed to the quantitative incorporation of Fe nanoparticles into atomized NIPAM-PDMS-doxorubicin (DOX) droplets. The Fe@NIPAM-PDMS-DOX nanocomposites released different amounts of DOX under a magnetothermal effect, which produced different levels of cytotoxic effects on the targeted HeLa cells. The thermosensitivity makes these nanocomposites an ideal candidate for important applications such as controlled drug delivery.

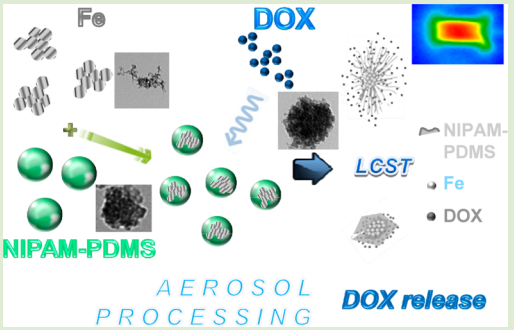

Nowadays, the use of nanoparticles as therapeutic and diagnostic agents is of interest owing to their unique properties such as their large specific capacity for drug loading, strong superparamagnetism, and efficient photoluminescence, among others.[1] For a nanoparticle delivery system, one challenge lies in successfully combining therapeutic agents, targeting treatments, and other desirable actions into one system; it is difficult to couple multiple functional groups in sufficient concentrations since the number of attachment sites on the particle surface is limited.[2] A magnetically targeted drug-delivery system involves binding a drug to small magnetic particles, injecting these into the bloodstream, and using a high gradient magnetic field to pull them out of suspension in the target region.

Of the smart polymeric materials, *N*-isopropylacrylamide (NIPAM) exhibits a lower critical solution temperature (LCST) of around 32 °C; theoretical efforts related to its thermosensitive behavior have been well-documented.[3,4] Many NIPAM-based hybrid material systems exist as colloidal liquids (mostly conducted using time-consuming batch wet chemical processes) with the presence of chemical cross-linkers,[5] which are generally stable for short periods of time. However, some of these systems are designed to be gradually degradable by hydrolysis, so long-term storage in liquid form is not a viable option for these types of systems.[6,7] One method to overcome the stability limitations of storing liquid formulations is to dry the formulation, allowing storage in a powder form. In contrast to classical wet chemical methods, aerosol-based processing requires far fewer preparation steps. It also produces material continuously, allows for a straightforward collection of particles, and generates low waste.[8]

Recently, more and more researchers have shown interest in thermosensitive nanocomposites. Such an inorganic−organic hybrid network made of NIPAM and incorporated inorganic nanoparticles will be very important in the multifunctionalization of novel high-performance nanocomposites.[9,10] Coating magnetic nanoparticles with NIPAM may lead to smart nanomaterials with dual sensitivity to magnetic field and temperature and is undoubtedly of interest for practical applications.[11,12] One possible approach is to use a hybridized carrier made with a magnetic core inside a thermally sensitive polymer micelle with a temperature-dependent drug release profile so that when the core is self-heated in response to an external magnetic stimulus it triggers the release of the drug contained within the micelle.[13,14] Most studies have incorporated NIPAM on the surface of magnetic nanoparticles using a layer-by-layer deposition technique. However, this procedure requires many steps when one wants to grow a polymer layer around the inorganic core.[15] Moreover, a previous report claimed that magnetic nanoparticles covered with water-soluble polymer may not be suitable as a drug carrier since the water-soluble system cannot survive at the blood circulation as they will readily dissolve in blood or biological fluids.[16]

This present work introduces a continuous aerosol-processed polydimethylsiloxane (PDMS)-conjugated iron (Fe)@NIPAM thermosensitive nanocomposite with different processing temperatures. The use of plasma discharges for nanoscale

Received: March 7, 2014
Accepted: March 31, 2014
Published: April 2, 2014

   dx.doi.org/10.1021/mz500142e | *ACS Macro Lett.* 2014, 3, 369−373

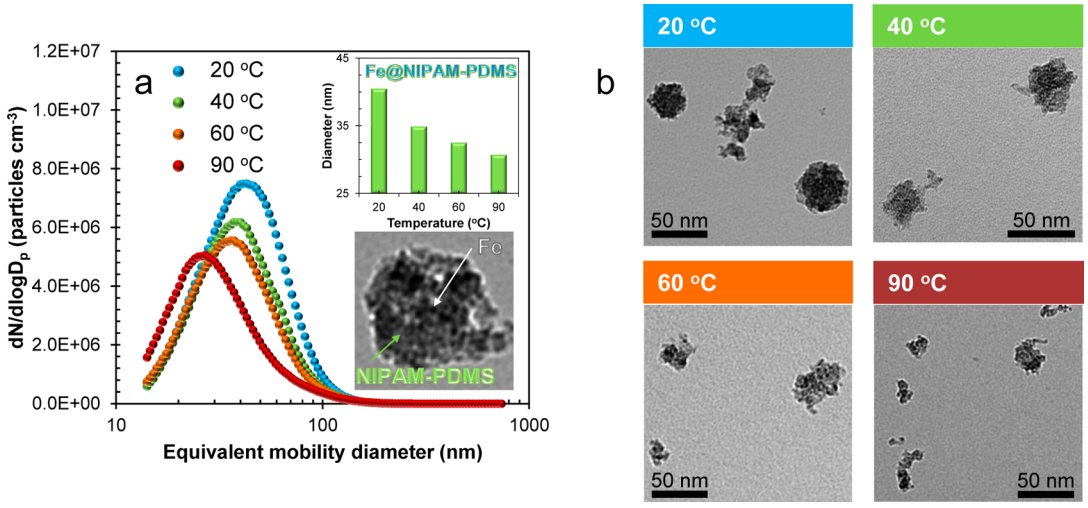

Figure 1. Aerosol-processed Fe@NIPAM-PDMS nanocomposites. (a) Size distributions of Fe@ NIPAM-PDMS nanocomposites with a high-magnification TEM image (inset) and (b) their morphologies (TEM images) with different temperatures in a heated tubular reactor. Standard deviations are noted in Table SI (Supporting Information).

materials synthesis is a rapidly developing field. In particular, nonthermal plasmas at atmospheric pressure are attractive because of several factors conducive to efficiency.[17] The cooling rate in the spark is defined from a previous study[18] and was −2900 K s^{-1} in the present case. In the present processing, the plasma-produced Fe nanoparticles were incorporated with NIPAM-PDMS components in the aerosol state. The water-soluble anticancer drug doxorubicin (DOX) was further loaded in the Fe@NIPAM-PDMS nanocomposites for investigation of the magnetothermally responsive drug release characteristics. DOX has been extensively used for the treatment of several forms of cancer. Recently, in some studies, DOX has been covalently linked to polymer carriers through a route of complicated organic syntheses due to their efficient use without high cytotoxicity.[19] The PDMS is an attractive polymer matrix due to its many favorable properties such as chemical inertness, biocompatibility, mechanical flexibility and stability, and most importantly its ease of processing.[20] It would be helpful not only to solve a predissolution issue of water-soluble components at biological fluids but also to enhance the entrapment of hydrophobic drugs. A spark discharge-produced Fe nanoparticle[21] and the particle-laden flow passed over a collison atomizer orifice where they mixed with the atomized NIPAM-PDMS-DOX solution to form hybrid droplets. The droplets then passed through a heated tube reactor, resulting in Fe@NIPAM-PDMS-DOX thermosensitive nanocomposites. The nanocomposites were separated using mechanical filtration, and finally they were employed as nanocarriers for a controlled release of DOX.

Thermosensitivity of Fe@NIPAM-PDMS nanocomposites was confirmed by a scanning mobility particle sizer (SMPS, TSI 3936, US; 4.6−163 nm detection range) in the gas phase with different temperatures ranging from 20 to 90 °C, as shown in Figure 1a. Briefly, when the Fe particles passed over the orifice of the collison atomizer, most Fe particles were encapsulated in the NIPAM-PDMS droplets, resulting in Fe@NIPAM-PDMS nanocomposites (Figure S1, Supporting Information). The ranges of the total number concentration (TNC), geometric mean diameter (GMD), and geometric standard deviation (GSD) of the Fe@NIPAM-PDMS nanocomposites were 2.40−3.81 × 10^6 particles cm^{-3}, 30.7−40.5 nm, and 1.55−1.59, respectively. Size distributions of individual spark-produced Fe and collison-atomized NIPAM-PDMS nanoparticles (a precursor of the whole nanoparticle) with different temperatures are described in the Supporting Information. The different temperatures were probably represented by different size distributions, in accordance with the following equations

$$\delta = \frac{V_p(T)}{V_{p0}} \propto \left(\frac{D_p(T)}{D_{p0}}\right)^3 \quad (1)$$

$$N \propto k_g\left(\frac{D_p}{\alpha D_{p0}}\right)^{d_f} \quad (2)$$

where δ is the size reduction parameter; $V_p(T)$ (or $D_p(T)$) and V_{p0} (or D_{p0}) are the volumes (or diameters) of the Fe@NIPAM-PDMS nanocomposites at temperature T in their fully swollen state;[22] N is the number of agglomerates: k_g is the fractal prefactor; D_{p0} is the size of a primary Fe@NIPAM-PDMS nanocomposite; and d_f is the fractal dimension. Although all the cases were investigated in the same solution concentration of NIPAM-PDMS, the concentrations and sizes of the measured nanocomposites varied according to their different degrees of morphological change (due to deswelling). The deswelling behavior of the nanocomposites is summarized in the inset of Figure 1a, where the morphology of the nanocomposites obtained by a transmission electron microscope (TEM, Libra 120, Carl Zeiss, Germany) is displayed as a function of the wall temperature of the heated tubular reactor (Figure 1b). The two different steps of particle reshaping, namely, incorporation (between Fe and NIPAM-PDMS) and morphological change, were identified. Even though the size of the nanocomposites normally increased at a higher temperature by thermal collision [$K_{col} = 4kT/3\mu$, where k is the Boltzmann factor and μ the gas viscosity], the average particle size decreased from 40.5 to 30.7 nm in the "coil-to-globule" transition.[23] This significant decrease in size between 20 and 40 °C was observed and showed that the temperature of the phase transition occurred around 30 °C. The shattered Fe nanoparticles were surrounded by the NIPAM-PDMS networks, and it appeared that the particles were dispersed throughout the

dx.doi.org/10.1021/mz500142e | ACS Macro Lett. 2014, 3, 369−373

NIPAM-PDMS matrix. The cross-linking points were probably formed via natural electrostatic positive charges[24] and/or interparticle termination of propagating radicals on the Fe particles[25] because there was no addition of chemical cross-linkers. As a result, the polymerization process could create a NIPAM-PDMS matrix around the Fe cores, which would grow thanks to the excess of NIPAM-PDMS networks formed during the incorporation. Similar phenomena are also represented in the different NIPAM-PDMS concentrations to synthesize other Fe@NIPAM-PDMS nanocomposites (Figure S2, Supporting Information). The lighter color in the structures represents the NIPAM-PDMS matrix, and the darker color represents the metallic Fe particles. These results indicate that temperature is a strong influence on the final nanocomposite morphology. From the TEM measurements, as shown in Figure 1b, the mean mode diameters for the 20 °C, 40 °C, 60 °C, and 90 °C cases were 51.2 ± 5.5, 38.8 ± 6.3, 34.1 ± 5.3, and 28.4 ± 4.6 nm, respectively, and these data were consistent with the SMPS data described in Figure 1a, which indicated that the heat treatment led to both a morphological change in the particle morphology and a decrease in the particle size. Penetration of the nanoparticles into the extracellular matrix of solid tumors is limited to particles smaller than 100 nm.[26] Therefore, the synthesized particles with a mean size of about <60 nm are suitable for further in vivo biological applications.

Nitrogen adsorption measurements (via a Micromeritics ASAP 2010 apparatus, US) with the Brunauer, Emmett, and Teller method were used to determine the porosity of the nanocomposites and to check the possibility of interconnected pores in the structures (Figure 2). The overall shapes of the

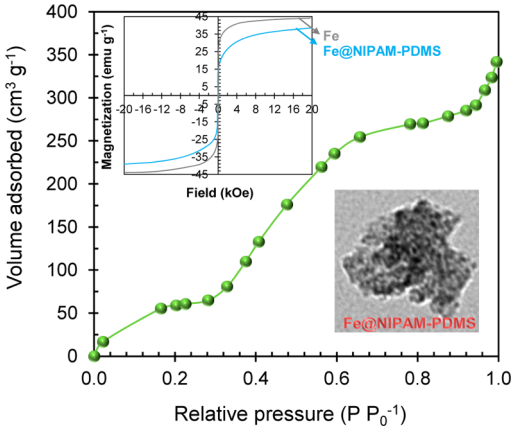

Figure 2. Adsorption isotherm of Fe@NIPAM-PDMS nanocomposites with a high-magnification TEM image (inset). Magnetization versus applied field curve of pure Fe nanoparticles and Fe@NIPAM-PDMS nanocomposites at 300 K is also displayed as another inset.

samples indicate their meso- and macroporous characteristics. The uptakes at >0.85 and <0.85 of $P\ P_0^{-1}$ may originate from the void spaces between agglomerated Fe@NIPAM-PDMS nanocomposites and voids within a Fe@NIPAM-PDMS nanocomposite (see inset TEM image of Figure 2), respectively. Another inset of Figure 2 shows magnetic hysteresis curves of the Fe@NIPAM-PDMS nanocomposites measured by a 7404 Lake Shore Cryotronics device (US) at 300 K. Magnetization intensity increases under the magnetic field, and thus superparamagnetic phenomena appear. The saturation magnetization of the Fe@NIPAM-PDMS nanocomposites was approximately 33 emu g^{-1}, and this low saturation magnetization value was less than that of the pure Fe nanoparticles (41 emu g^{-1}). This can be explained by considering the diamagnetic contribution of the NIPAM-PDMS layers surrounding the Fe particles. It is possible that surface magnetic anisotropy was changed with the existence of NIPAM-PDMS networks. The surface spin disorientation increased, and thus the magnetic moment decreased.

As shown in Figure 3a, Fe@NIPAM-PDMS-DOX hybrid droplets were formed by incorporating Fe@NIPAM-PDMS

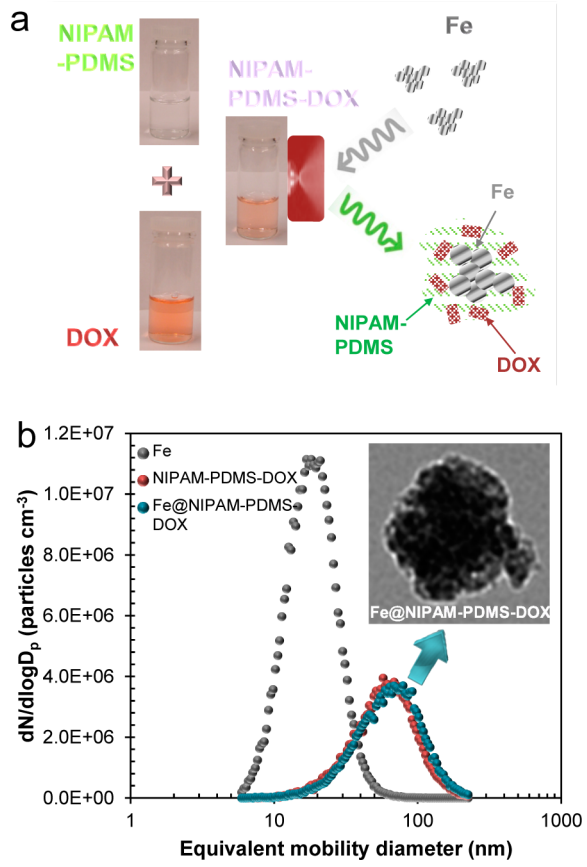

Figure 3. Aerosol-processed Fe@NIPAM-PDMS-DOX nanocomposites. (a) Schematic diagram of the assembly of Fe@NIPAM-PDMS-DOX in the aerosol state. (b) Size distributions of spark-produced Fe nanoparticles, collison-atomized NIPAM-PDMS-DOX droplets, and their hybridized structures, Fe@NIPAM-PDMS nanocomposites, with a high-magnification TEM image (inset).

with DOX during the aerosol processing, in which the concentrations of DOX ranged from 0.2 to 2.0 μg mL^{-1}. We further verified the incorporation of the Fe@NIPAM-PDMS with the DOX drug by measuring the size distributions of the NIPAM-PDMS-DOX and Fe@NIPAM-PDMS-DOX cases in the aerosol state. The TNC, GMD, and GSD of the Fe@NIPAM-PDMS-DOX nanocomposites were 2.01 × 10^6 particles cm^{-3}, 61.8 nm, and 1.69, respectively. The analogous data for NIPAM-DOX droplets were 1.96 × 10^6 cm^{-3}, 57.3 nm, and 1.67, respectively. The size distribution of the Fe@NIPAM-PDMS-DOX was rather similar to the NIPAM-PDMS-DOX droplets compared to that of the Fe particles, and there was no bimodal distribution character, implying that nearly all Fe particles were incorporated with the NIPAM-PDMS-DOX, to form Fe@NIPAM-PDMS-DOX nanocomposites. The inset of Figure 3b shows a TEM image of the Fe@NIPAM-PDMS-

dx.doi.org/10.1021/mz500142e | ACS Macro Lett. 2014, 3, 369−373

DOX nanocomposites, which shows a darker color than the Fe@NIPAM-PDMS nanocomposite owing to further incorporation of DOX in a Fe@NIPAM-PDMS platform. Further measured hydrodynamic diameters of both Fe@NIPAM-DOX nanocomposites with and without PDSM using a zetasizer (Nano Z, Malvern Instruments, U.K.) were 55.4 ± 9.8 nm and 4.7 ± 2.5 nm, respectively, which imply that PDMS incorporation did retard a dissolution of NIPAM and/or DOX.

Figure S3 (Supporting Information) shows the Fourier transform infrared spectra of Fe@NIPAM-PDMS, Fe@DOX, and Fe@NIPAM-PDMS-DOX samples. The absorption peak at 3293 cm^{-1} can be attributed to the stretch of the hydrogen-bonded N−H group. The asymmetric stretching vibration of the CH_3 group occurs at 2973 cm^{-1}; the secondary amide C═O stretching shows a strong band at 1650 cm^{-1}; and the asymmetric bending deformation of CH_3 groups on isopropyl ($-CH(CH_3)_2$) occurs at 1461 cm^{-1}.[3] This sample also shows a characteristic band of the Si−O−Si stretching (inset of Figure S3, Supporting Information) of PDMS at 800−1100 cm^{-1}. Fe@DOX showed a characteristic IR absorption band at 1734 cm^{-1} due to the stretching vibration of the carbonyl group at the 13-keto position and bands at 1614, 1585, and 1414 cm^{-1} due to the stretching vibration of two carbonyl groups of the anthracene ring of the DOX molecule, and the peak at 1545 cm^{-1} is due to the stretching bands of the N−H group.[27] In addition, the broad band near 3327 cm^{-1} refers to the vibration of the −OH groups with a contribution of $-NH_2$ within this band. These characteristic bands remained as they were incorporated with NIPAM-PDMS, which demonstrates the successful DOX conjugation on the Fe@NIPAM-PDMS nanocomposites in the single-pass process, and also implied that the DOX indeed can be physically absorbed within the nanocomposite networks. The characteristic bands of NIPAM at 2972 cm^{-1} confirmed that the NIPAM chains existed in the nanocomposites. We also measured the zeta potentials of the nanocomposite dispersion in pH 7.3 phosphate-buffered saline (PBS) buffer to be 2.2 ± 0.7 mV; this positive charge indicates that the nanocomposites are electrophysiologically capable of binding to negatively charged proteins.

We verified the temperature increase of the nanocomposites in an alternating electromagnetic field (360 kHz and 6.5 kA m^{-1}). The experiment was performed in a glass tube thermoinsulated with a concentration of 10 mg mL^{-1} of the nanocomposites placed in the center of the coil. The temperature increased steadily for 1 h until it reached about 40 °C, indicating a promising behavior for the hyperthermia treatment. When superparamagnetic nanocomposites are placed in the magnetic field, the total energy dissipated P to heat is calculated as

$$P = \frac{\mu_0 \chi_0 H^2 \omega^2 \tau}{2\tau(1 + \omega^2 \tau^2)} \quad (3)$$

where χ_0 is the equilibrium susceptibility of the magnetic nanocomposites, and ω is the applied frequency of the magnetic field. τ and μ_0 are the effective relaxation time and magnetic permeability, respectively, and H is the intensity of the magnetic field.

The DOX cumulative release results are shown in Figure 4a. In PBS solution at pH 7.3 in 24 h, the cumulative release amounts of DOX from Fe@NIPAM-PDMS-DOX nanocomposites were approximately 49% and 14% at 25 and 37 °C, respectively. This indicates that Fe@NIPAM-PDMS-DOX

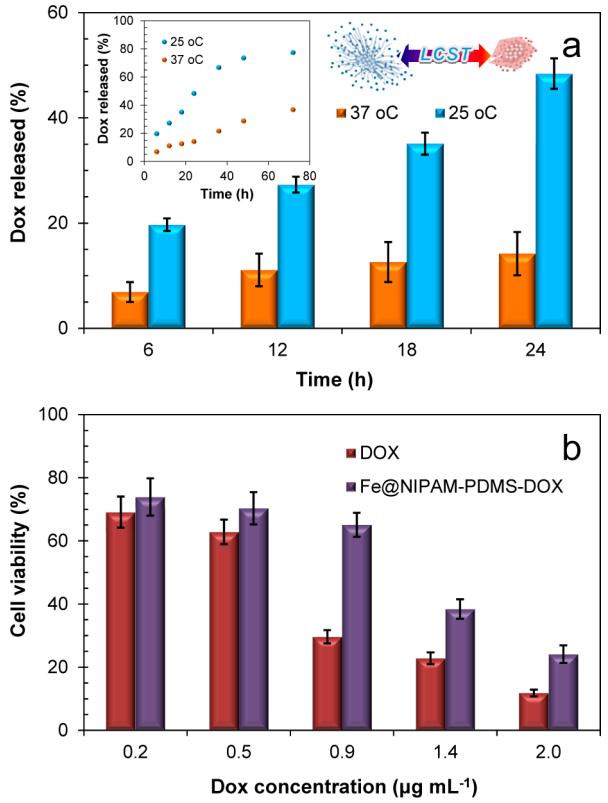

Figure 4. In vitro measurements of DOX release and cytotoxic activity against HeLa cells. (a) DOX release profiles from Fe@NIPAM-PDMS-DOX nanocomposites with different temperatures. The long-term DOX release and mechanism of DOX release are also displayed as the inset. (b) Activity of Fe@NIPAM-PDMS-DOX nanocomposites against HeLa cells. MTT assay showing viability of HeLa cells after 24 h.

nanocomposites possess thermosensitive DOX release behaviors, and the cumulative release amount was higher at 25 °C than at 37 °C. It can be explained that NIPAM-PDMS chains are in collapsed and hydrophobic conformations at 37 °C above the LCST, which can retard DOX release as shown in the inset of Figure 4a. Measurements of a long-term DOX release (inset of Figure 4a) at 25 and 37 °C reached approximately 77% and 37%, respectively, which are consistent with the 24 h measurements. The lower DOX release at physiological temperature is advantageous as it can be anticipated that lesser DOX might be lost during circulation.[28] To assess the DOX delivery potential of the nanocomposites and the anticancer activity of the released DOX, in vitro cytotoxicity assays were performed by a 3-(4,5-dimethylthiazol-2-yl)-2,5-diphenyltetrazolium bromide (MTT) assay against a HeLa cell line at different administered concentrations of DOX ranging from 0.2 to 2.0 μg mL^{-1}. To compare the cytotoxic activity of the nanocomposite with that of the free DOX, the free DOX was used as a control. The HeLa cell proliferation results are shown in Figure 4b. For comparison purposes, the cytotoxicity of the Fe@NIPAM-PDMS nanocomposites shows that that the range of average cell viability with different mass concentrations of 5−100 μg mL^{-1} was 94 ± 4.12%−80 ± 5.18%, which implies that nanocomposites without DOX may be nontoxic under standard cell culture conditions. It was found that the free DOX exhibits higher inhibition on HeLa cells in 24 h compared with the loaded DOX at the same DOX concentration when it is more than about 0.9 μg mL^{-1}. The dose required for 50% cellular

dx.doi.org/10.1021/mz500142e | ACS Macro Lett. 2014, 3, 369−373

growth inhibition of the nanocomposites is about 0.85 μg mL^{-1}, which is higher than that of the free DOX (~0.55 μg mL^{-1}). The results are most likely related to the slow release of the DOX from the nanocomposites in the course of incubation. This proves that the nanocomposites can delay DOX release. A possible reason is that more compact structures result in a lower diffusion rate of DOX molecules after loading of DOX in the Fe@NIPAM-PDMS platforms retards the cytotoxic effect of DOX on the cells. Because of slower DOX release, the system may be suitable at the blood circulation as they will readily dissolve in blood or biological fluids. As a drug-delivery system, the Fe@NIPAM-PDMS-DOX nanocomposites are beneficial to control the side effects of DOX on cells.

We developed the aerosol processing to self-assemble Fe@NIPAM-PDMS-DOX nanocomposites for a controlled DOX release. DOX as an anticancer drug model was loaded into the Fe@NIPAM-PDMS platforms, and the DOX release was performed in a PBS solution at 25 and 37 °C. The results verify that Fe@NIPAM-PDMS nanocomposites as drug nanocarriers show thermosensitive DOX release behaviors. Furthermore, MTT assays of Fe@NIPAM-PDMS-DOX nanocomposites against HeLa cells confirm that the Fe@NIPAM-PDMS-DOX nanocomposites can be used for a controlled drug release. This nanocomposite design approach provides useful insights for designing and improving the applicability of nanocomposites for the development of smart drug delivery and controlled release systems.

■ ASSOCIATED CONTENT

Supporting Information

Schematic diagram of Fe@NIPAM-PDMS nanocomposites synthesis, size distributions and morphologies of individual Fe and NIPAM-PDMS nanoparticles, size distributions and morphologies of Fe@NIPAM-PDMS nanocomposites, and FTIR spectra and zeta potentials. This material is available free of charge via the Internet at http://pubs.acs.org.

■ AUTHOR INFORMATION

Corresponding Authors

*Tel.: +1-765-494-5499. E-mail: jbyeon@purdue.edu.
*Tel.: +82-41-540-5925. Fax: +82-41-540-5929. E-mail: jwkim@hoseo.edu.

Notes

The authors declare no competing financial interest.

■ REFERENCES

(1) Baeza, A.; Guisasola, E.; Ruiz-Hernández, E.; Vallet-Regí, M. *Chem. Mater.* **2012**, *24*, 517−524.
(2) Fan, J.; Fang, G.; Zeng, F.; Wang, X.; Wu, S. *Small* **2013**, *9*, 613−621.
(3) Li, P.; Zhu, A. M.; Liu, Q. L.; Zhang, Q. G. *Ind. Eng. Chem. Res.* **2008**, *47*, 7700−7706.
(4) Balasubramaniam, S.; Pothayee, N.; Lin, Y.; House, M.; Woodward, R. C.; St. Pierre, T. G.; Davis, R. M.; Riffle, J. S. *Chem. Mater.* **2011**, *23*, 3348−3356.
(5) Chen, T.; Cao, Z.; Guo, X.; Nie, J.; Xu, J.; Fan, Z.; Du, B. *Polymer* **2011**, *52*, 172−179.
(6) Park, J.-H.; Lee, Y.-H.; Oh, S.-G. *Macromol. Chem. Phys.* **2007**, *208*, 2419−2427.
(7) Bulmus, V.; Chan, Y.; Nguyen, Q.; Tran, H. L. *Macromol. Biosci.* **2007**, *7*, 446−455.
(8) Pratsinis, S. E. *AIChE J.* **2010**, *56*, 3028−3035.
(9) Zhang, S.; Zhang, L.; He, B.; Wu, Z. *Nanotechnology* **2008**, *19*, 325608.
(10) Leal, M. P.; Torti, A.; Riedinger, A.; Fleur, R. L.; Petti, D.; Cingolani, R.; Bertacco, R.; Pellegrino, T. *ACS Nano* **2012**, *6*, 10535−10545.
(11) Li, Q.; Zhang, L.; Bai, L.; Zhang, Z.; Zhu, J.; Zhou, N.; Cheng, Z.; Zhu, X. *Soft Matter* **2011**, *7*, 6958.
(12) Luo, B.; Song, X.-J.; Zhang, F.; Xia, A.; Yang, W.-L.; Hu, J.-H.; Wang, C.-C. *Langmuir* **2010**, *26*, 1674−1679.
(13) Liu, T.-Y.; Liu, K.-H.; Liu, D.-M.; Chen, S.-Y.; Chen, I.-W. *Adv. Funct. Mater.* **2009**, *19*, 616−623.
(14) Li, J.; Qu, Y.; Ren, J.; Yuan, W.; Shi, D. *Nanotechnology* **2012**, *23*, 505706.
(15) Laurenti, M.; Guardia, P.; Contreras-Cáceres, R.; Pérez-Juste, J.; Fernandez-Barbero, A.; Lopez-Cabarcos, E.; Rubio-Retama, J. *Langmuir* **2011**, *27*, 10484−10491.
(16) Shen, J.-M.; Yin, T.; Tian, X.-Z.; Gao, F.-Y.; Xu, S. *ACS Appl. Mater. Interfaces* **2013**, *5*, 7014−7024.
(17) Ostrikov, K.; Neyts, E. C.; Meyyappan, M. *Adv. Phys.* **2013**, *62*, 113−224.
(18) Byeon, J. H.; Kim, J.-W. *Appl. Phys. Lett.* **2010**, *96*, 153102.
(19) Bahadur, K. C. R.; Xu, P. *Adv. Mater.* **2012**, *24*, 6479−6483.
(20) Li, D.; Li, C.; Wang, A.; He, Q.; Li, J. *J. Mater. Chem.* **2010**, *20*, 7782−7787.
(21) Byeon, J. H.; Kim, J.-W. *Appl. Phys. Lett.* **2012**, *101*, 023117.
(22) Karg, M.; Hellweg, T. *Curr. Opin. Colloid Interface Sci.* **2009**, *14*, 438−450.
(23) Lian, X.; Jin, J.; Tian, J.; Zhao, H. *ACS Appl. Mater. Interfaces* **2010**, *2*, 2261−2268.
(24) Byeon, J. H.; Kim, J.-W. *Langmuir* **2010**, *26*, 11928−11933.
(25) Czaun, M.; Hevesi, L.; Takafuji, M.; Ihara, H. *Chem. Commun.* **2008**, *18*, 2124−2126.
(26) Goodman, T. T.; Olive, P. L.; Pun, S. H. *Nanomedicine* **2007**, *2*, 265−274.
(27) Chouhan, R.; Bajpai, A. K. *J. Nanobiotechnol.* **2009**, *7*, 5.
(28) Rastogi, R.; Gulati, N.; Kotnala, R. K.; Sharma, U.; Jayasundar, R.; Koul, V. *Colloid Surf. B: Biointerfaces* **2011**, *82*, 160−167.